PIEZORESISTIVE CHARACTERISTICS OF SILICON CARBIDE FOR INTEGRATED SENSOR APPLICATIONS

Pooran Joshi, Tolga Aytug, Shannon Mahurin, Richard Mayes, Sacit Cetiner, Hong Wang, Ivan Kravchenko, Yanwen Zhang, Anton Ievlev, and Roger Kisner
Oak Ridge National Laboratory, 1 Bethel Valley Rd, Oak Ridge, TN 37830
joshipc@ornl.gov

Lauren Nuckols
Department of Materials Science and Engineering, The University of Tennessee, Knoxville, TN 37996

ABSTRACT

Successful ubiquitous deployment of advanced reactors will depend to a large extent on the development of high-performance materials and sensors. Recently, there has been increasing interest in advanced reactors operating at very high temperatures (greater than 700 °C) and using molten salts as the primary coolant. In such reactor systems, temperature and pressure measurements are conducted using standard legacy thermocouples and pressure measurement technologies, both of which suffer from resolution issues, inaccuracies, and drift under harsh operating temperature and radiation conditions. We report on the structural, electrical, and mechanical characteristics of SiC materials and devices for the development of an integrated monolithic sensor unit capable of simultaneously monitoring temperature, pressure and flow in molten salt reactors, while at the same time exhibiting significant improvements in resolution, accuracy and signal-to-noise ratio.

Wide bandgap and chemical inertness of SiC make it suitable for harsh environment sensor applications. We report on the development of a SiC pressure sensor exploiting its piezoresistive properties. Attempts have been made to fabricate thermally stable pressure sensor through doping induced high gauge factor. Both implanted and in-situ doped SiC wafers are being investigated to analyze the impact of dopant type and concentration on the piezoresistive characteristics. The microstructure, composition, and electrical conductivity of SiC samples have been analyzed to find optimum dopant incorporation and activation conditions. The mechanical measurements are being conducted on SiC beams with photolithographically defined surface piezoresistors to establish gauge factor for high performance sensors that can operate at temperatures beyond the limits of conventional silicon CMOS materials and devices.

Key Words: Silicon Carbide, Implantation, Piezoresistor, Sensor, Thin Film

1 INTRODUCTION

Robust and non-intrusive pressure sensors have been identified as technology gap for advanced reactors, particularly for molten salt and sodium fast reactors [1, 2]. Materials based on appropriately-doped SiC offer a method to address the problems of drift, accuracy and resolution associated with current legacy instrumentation used in the harsh environment of advanced reactors. In fact, silicon carbide is being considered for a variety of nuclear reactor components due to its outstanding physical and chemical properties, including high thermal conductivity, high temperature stability, chemical inertness, extreme hardness and small neutron capture cross-section [3, 4]. The unique electronic properties of SiC make it the semiconductor material of choice for high temperature, high power, and high frequency applications. As is the focus of the present investigation, an integrated temperature and pressure sensor can be assembled on the same encapsulated substrate of SiC by appropriately doping selective areas to form p-n junctions, Schottky diodes, and piezoresistive sensing regions [5, 6]. The present study is focused on the implantation of dopants in 6H- and 3C-SiC wafers and understanding the dopant profile, thermal activation and electrical

conductivity characteristics. Semi-insulating SiC wafers are suitable to define isolated sensors and devices through local implantation of the suitable n-type and p-type species. The device development effort is focused on in-situ doped 3C-SiC wafers to analyze the impact of doping at high concentration levels exceeding 1×10^{17} cm^{-3}.

2 EXPERIMENTAL

The piezoresistive sensor development effort was focused on ion-implantation of undoped 6H- and 3C-SiC wafers to analyze the impact of doping concentration and activation anneal on the microstructure and electrical characteristics. The dopant profile was established by Stopping and Range of Ions in Matter (SRIM) simulator and confirmed by time-of-flight secondary ion mass spectrometry (ToF-SIMS) and Rutherford backscattering spectroscopy (RBS) techniques. The microstructure and surface morphology were analyzed by x-ray diffraction (XRD) and atomic force microscopy (AFM) techniques. The electrical characteristics of the films were measured by Ecopia HMS-3000 Hall effect measurement system and four-point probe technique using SRM-232 surface resistivity meter. The device development effort focused on piezoresistive element patterning on in-situ doped 3C-SiC films. The mechanical measurements were conducted on SiC piezoresistors defined on 3C-SiC/Si beam. The details of implantation study and piezoresistive device development are discussed in the following sections.

3 RESULTS AND DISCUSSION

3.1 Ion-Implantation and Dopant Profile

We used SRIM, a Monte Carlo ion transport simulation tool to predict concentration-depth profiles in a material as a function of incident ion species, dose, and beam energy. Looking at the silicon technology, typical piezoresistor dose ranges from 1×10^{14} to 5×10^{16} ions/cm^2 with energy distribution in the range of 30-150 keV [7] while even lower implantation energies have been reported for electronic device fabrication on SiC [8]. In the present work, the implantation simulation was performed with a 7º tilt to avoid ion channeling. For the target SiC material, a series of simulations were performed to determine an acceptable implantation scheme to achieve the 500-Å-wide plateau. To have a reasonably flat distribution and achieve a high piezoresistive coefficient, the simulation work focused on multiple implants at different dose and energy levels to achieve a uniform profile. The first set of SiC samples were implanted, as highlighted in Fig. 1(a), at 1.0×10^{15} N ions/cm^2 at 10 keV, 2.0×10^{15} N ions/cm^2 at 20 keV, and 2.5×10^{15} N ions/cm^2 at 25 keV with the target projected ranges of about 20, 30, and 50 nm, respectively. The composite profile indicated a peak concentration in the range of 20-50 nm.

The ToF-SIMS measurements were conducted on 6H-SiC to verify the dopant profile, and chemical composition on the surface and in the bulk of the sample. Measurements were carried out using two focused ion beams: (1) Bi_3^+ ion beam (30 keV energy, 30 nA current, 5 µm spot size) was used as a primary source for extraction of the secondary analyte ions; (2) Cs^+ ion beam (1 keV energy, 43 nA current, 20 µm spot size) was used as a sputtering source for removing the surface layers of the sample for the depth profiling. Extracted ions were analyzed using time-of-flight mass analyzer in negative ion detection mode, which allowed detection of ions with mass up to 500 u and mass resolution $m/\Delta m = 3{,}000 – 10{,}000$. Measurements were run in non-interlaced mode, where every chemical analysis scan by Bi_3^+ source (raster size 100 × 100 µm) was followed by sputtering with Cs^+ (raster size 300 × 300 µm), which allowed chemical analysis as a function of depth down to 127 nm. In this approach, mass spectra are collected from every layer to analyze chemical changes in the bulk with selected peaks corresponded to O^-, C^-, Si^- and CN^- ions as shown in Fig. 1(b). Area of those peaks were plotted as a function of sputter time and further calibrated to depth using atomic force microscope (AFM) in the same vacuum chamber. AFM profiling of the resulted sputtering craters showed sputter rate of about 2.8 nm/min. The nitrogen depth profile was evaluated by tracking CN^- fragments as in SiC the atomic nitrogen exhibits low ion yield and the interference from carbon-hydrogen

peaks is strong. As shown in Fig. 1(b), the nitrogen penetration depth in the sample is about 90 nm while a peak concentration is achieved at a depth of about 40 nm which is consistent with the SRIM analysis.

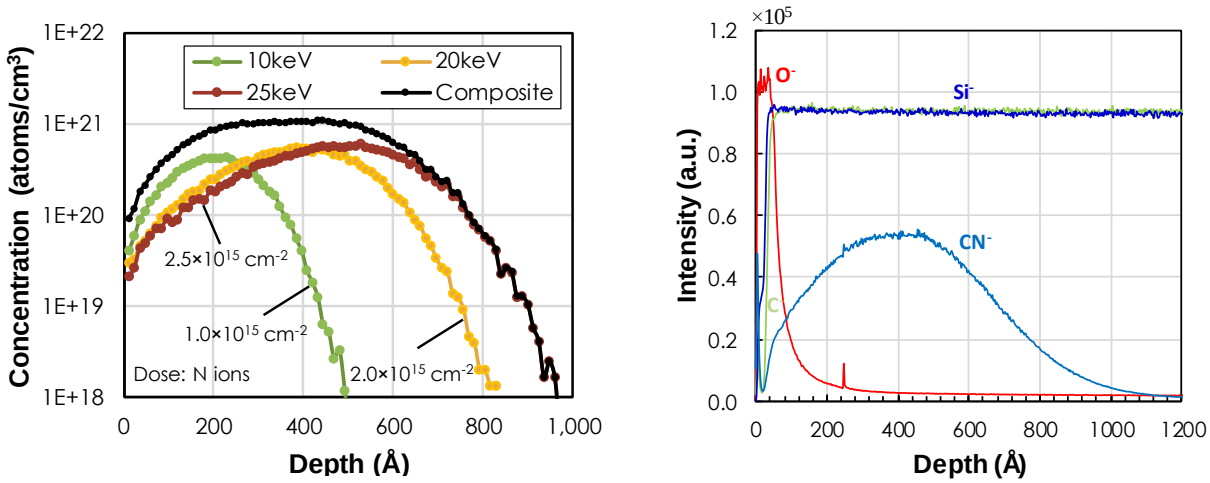

(a) (b)

Figure 1. Dopant profile in 6H-SiC as established by (a) SRIM simulation and (b) SIMS measurements.

Rutherford backscattering spectroscopy (RBS) in random and channeling geometry (RBS/C) is a sensitive technique to determine crystal quality, surface oxidation, or damage in crystalline samples resulting from implantation or other doping techniques as used in this work. RBS was conducted in channeling configuration at room temperature using a well-collimated parallel beam of 2.0 MeV He ions and a backscattering angle of 168° which is optimized for both mass and depth resolutions [9]. RBS measurements were conducted on 6H-SiC samples annealed in the range of 1100-1450 °C. Both the virgin spectrum and the annealed spectra for 6H-SiC show a low backscattering yield with the yield of Si surface peaks at ~ 50 counts for the pristine sample, at ~110 counts for 1100 °C and 1450 °C treated samples, and at ~220 for the 1300 °C sample. The backscattering yield from the 6H-SiC sample, annealed at 1100°C, in a random direction is above 700 counts as shown in Fig. 2(a). The low yield from all the annealed samples indicates that crystallinity is well-preserved. While no oxygen signal is observed in the pristine sample, oxygen signal from surface oxidation is clearly observable at around channel 700 for all the annealed samples. Detailed analysis (e.g., as shown in Fig. 2(a) by fitting the random spectra from the 1100 °C sample) suggests a growth of surface oxidation layer with a thickness of about 3.5, 13.8, and 7.2 nm on 1100 °C, 1300 °C and 1450 °C annealed samples, respectively. The random RBS spectrum of 3C-SiC sample annealed at 1100 °C is shown in Fig. 2(b). Compared to 6H-SiC samples, the RBS spectrum of 3C-SiC sample shows a much higher yield and wider peaks of backscattered He signals resulting from Si and O in the surface region. A surface oxidation layer of 33.9 nm is determined from the simulation shown in Fig. 2(b). Detailed experiments are being conducted to analyze the impacts of furnace test setup and 3C-SiC wafer type and doping on the oxide growth.

SIMNRA was used for the simulation of nitrogen profile in 1100°C treated 6H-SiC. Based on the simulation, the nitrogen signal should appear on top of the Si signal. However, the expected low count of the nitrogen peak is likely concealed within the experimental data uncertainty [10]. Nitrogen content was also not detected during channeling RBS, where the backscattering from the host material is greatly reduced making the detection of impurities that are implanted on interstitial sites of the SiC lattice more probable. The channeling RBS results may be indicative that nitrogen implants itself as substitutional defects in the silicon carbide matrix displacing the host atoms.

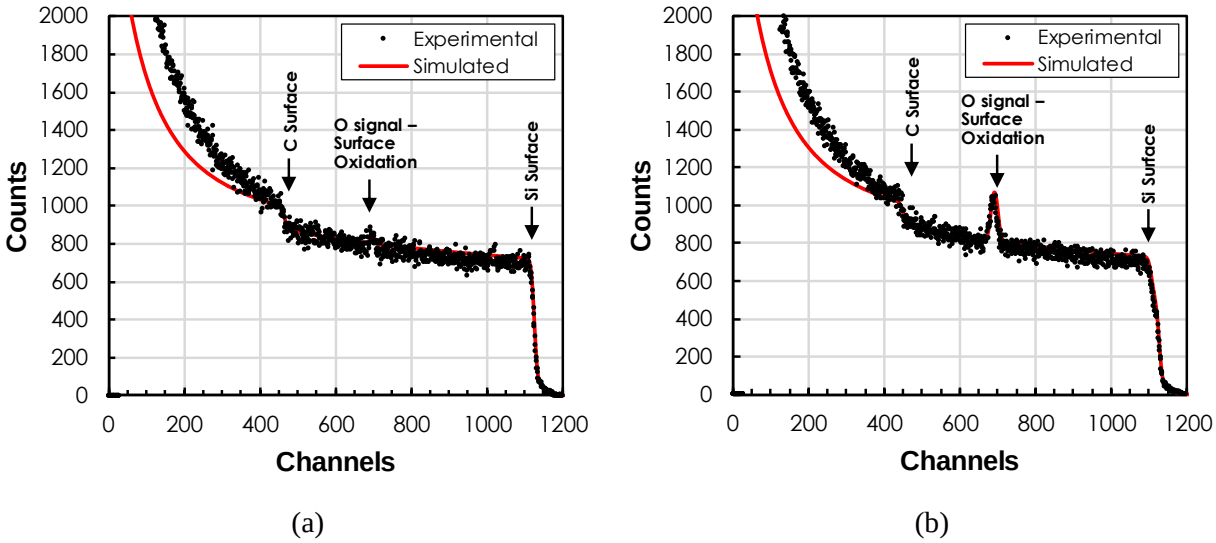

Figure 2. (a) Random spectrum from the 1100 °C treated (a) 6H-SiC and (b) 3C-SiC samples together with the simulation (solid red line).

To gain an understanding of the impact of high temperature implants on the 6H- and 3C-SiC lattice disorder, the depth profiles of relative Si disorder from the 1100°C treated 6H- and 3C-SiC samples are determined, as shown in Fig. 3, from the RBS spectra using an iterative procedure [11]. Both the samples showed a low disorder after implantation at a temperature of 600 °C. However, a higher disorder level, peaking at 11%, is observed in the 3C-SiC sample, as compared with ~4% disorder in 6H-SiC sample. The disorder level will be tracked for the various SiC polytypes as we optimize the doping concentration to achieve high gauge factor in piezoresistive sensors.

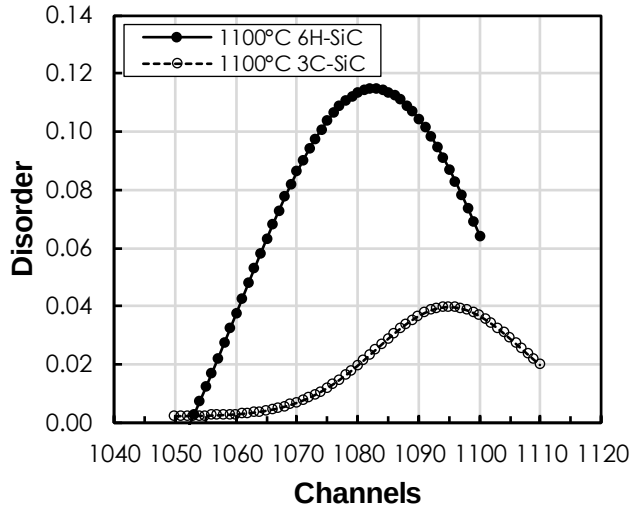

Figure 3. Depth profiles of relative Si disorder from the 1100°C treated 6H-SiC and 3C-SiC samples.

3.2 Microstructure and Surface Morphology

X-ray diffraction patterns were collected on a PANalytical Empyrean diffractometer with Ni-filtered Cu K_α (λ = 1.54 Å) radiation operating at 45 kV and 40 mA. Each scan was 20 min and covered a 2θ range of 10-90°. For ion-implanted SiC annealing, the samples were placed in an alumina boat and inserted into a quartz tube in a tube furnace (MTI, GSL1800S). The samples were evacuated overnight at a base pressure of 6 millitorr (mTorr). During the annealing process, high purity argon flowed through the tube in order to achieve a pressure of 75 millitorr. Prior to entering the tube furnace, the argon flowed through an oxygen scrubber to reduce the oxygen content. A zirconium sponge was also inserted into the tube close to the SiC sample to further reduce the oxygen content. The sample was then heated to the target temperature at a rate of 10 °C/min and then remained at the target temperature for 1 hour before cooling down to room temperature.

Figure 4 shows XRD patterns for the pure, implanted and annealed SiC samples. For 6H-SiC samples, the most prominent peaks occur at approximately 2θ=35.7° and 75.5° which correspond to the (006) and (0012) planes, respectively [12]. The N-implantation did not shift the peak appreciably indicating little effect on the crystal structure of the SiC. Annealing at 1100 °C caused a slight shift of approximately 0.2° to lower angle (2θ) for both the (006) and (0012) peaks which could be due to changing surface roughness. The peak position shifted further left at an annealing temperature of 1300 °C indicating an increase in lattice parameter. As the annealing temperature was increased to 1440 °C, the peak position shifted back to the original position of the pure 6H-SiC which may be due to an increase in the compressive residual stress. The widths of the peaks did not change significantly with annealing temperature which indicates that the grain size did not change during the annealing process; however, the intensity of the peaks at the highest annealing temperature was substantially reduced possibly due to increase in the oxide layer thickness on the surface as established by the RBS analysis. The 3C-SiC sample showed an intense XRD peak corresponding to (200) plane [13]. The 3C-SiC samples showed an increase in (200) peak intensity and a left shift after annealing at 1100 °C indicating an increase in the lattice constant.

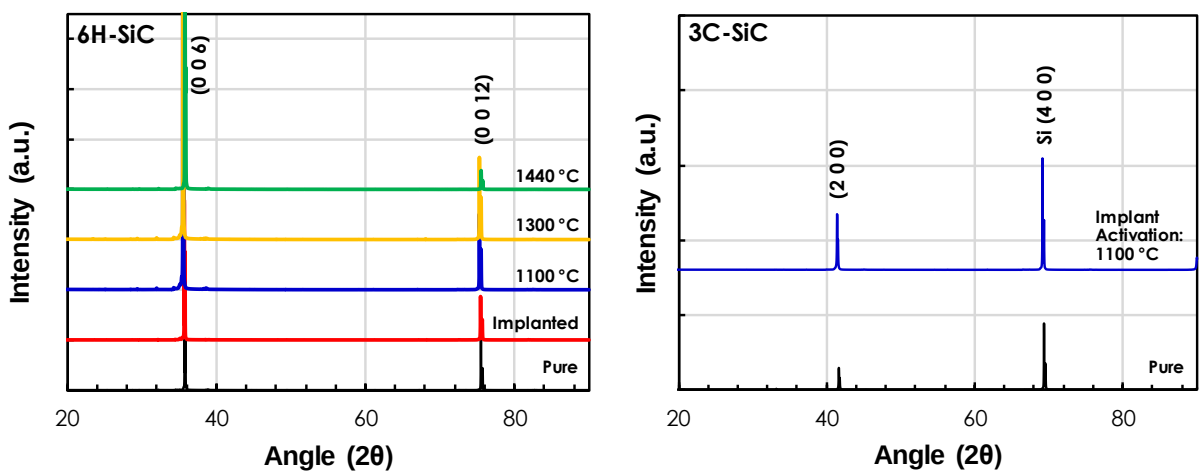

(a) (b)

Figure 4. XRD patterns for (a) 6H-SiC and (b) 3C-SiC for the pure, implanted and annealed samples.

Atomic force microscopy in tapping mode was employed to examine the surface morphology of the SiC samples after annealing at different temperatures for dopant activation. AFM images were acquired at room temperature by Nanoscope III atomic force microscope using commercial Si probes with a high resonance frequency of 300 kHz. Figures 5 shows the surface morphologies of pristine 6H- and 3C-SiC wafers before annealing and after the N_2 implantation followed by thermal treatment. After the implantation, the 6H-SiC and the 3C-SiC samples were electrically activated by annealing at 1450 °C and

1100 °C, respectively, for 60 min under 6 mTorr vacuum ambient. Vicinal surface steps oriented in the < 00-10 > direction, associated with the substrate miscut, are observed for the 6H-SiC wafer (Fig. 5(a1)). After the heat treatment, a significant increase in the width of the surface terraces for the 6H-SiC (Fig. 5(a2)) and nucleation of triangular defects with an obtuse-angled structure were realized on the surfaces of 6H-SiC samples. Previous studies documented that these particles have 3C-SiC nature and the origins of which are related to the presence of foreign particles and substrate defects (e.g., scratches) [14]. We also found that surface coarsening increased with temperature. In fact, the enlarged width of the terraces for the 6H-SiC and the formation of step-bunching in the case of 3C-SiC films (Fig. 5(b2)) are a result of surface vaporization of the Si-containing molecules from SiC (Si sublimation) and re-accumulation on the surface during thermal treatments at temperatures greater than 1400 °C, as observed in earlier studies [15]. In comparison to the as-implanted samples, the average surface roughness (Ra) value increased from 0.3 nm to 1.9 nm for 6H-SiC, 1.9 nm to 3.1 nm for 3C-SiC/Si samples. Note that nitrogen implantation did not have a significant effect on the Ra values, indicating that the observed increase in roughness is a consequence of the modifications in the surface morphologies after the thermal treatments.

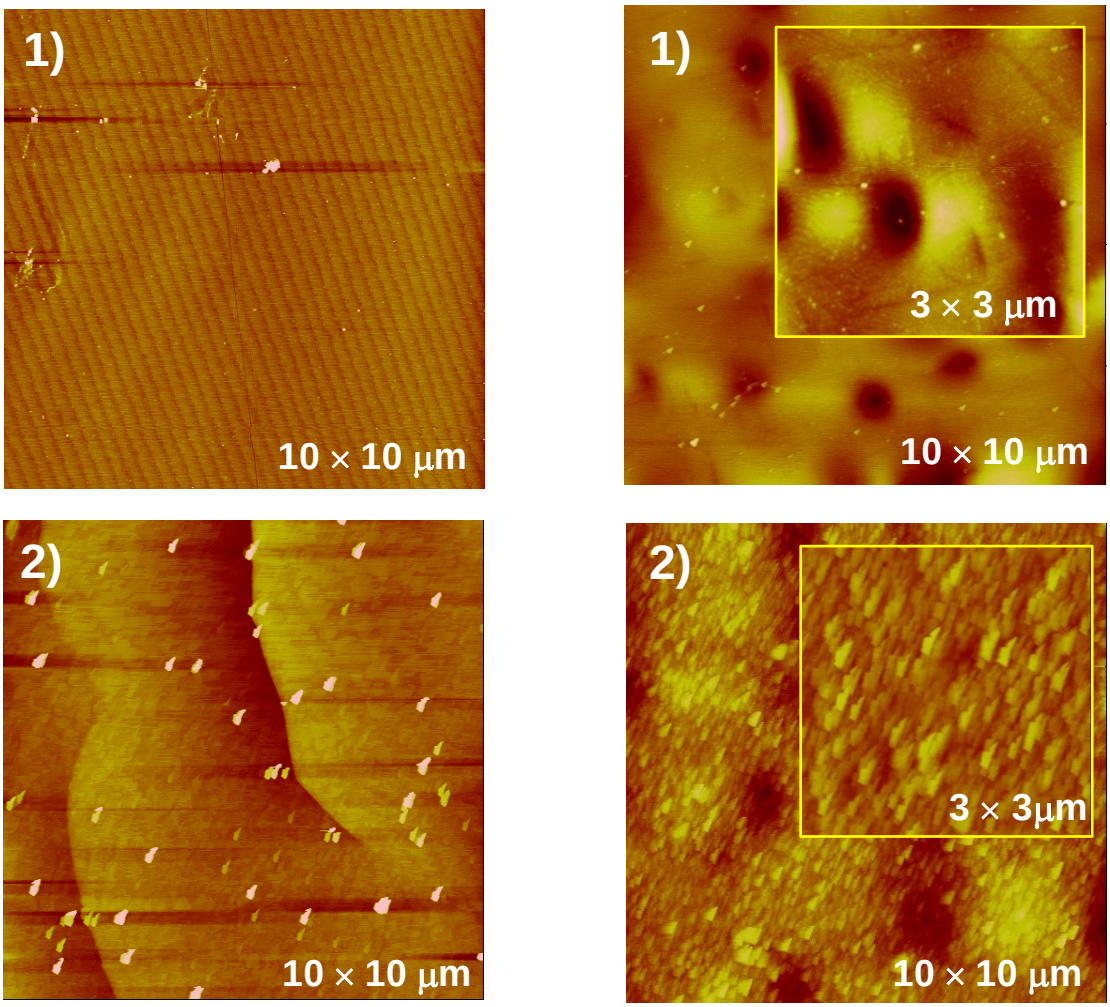

(a) (b)

Figure 5. AFM images of (a) 6H-SiC and (b) 3C-SiC/Si (1) before and (2) after annealing at 1450 °C/60 min and 1100 °C/60 min, respectively.

3.3 Electrical Characteristics

Electrical characteristics of the doped 6H- and 3C-SiC samples were evaluated after annealing to analyze the impact of the activation temperature. The carrier concentration and the mobility of the samples were established by room temperature Hall effect measurements. The Hall effect measurements were conducted on square samples using indium contacts. The electrical conductivity of the samples was measured in terms of the sheet resistance after activation anneal. The sheet resistance of the films was measured by four-point probe technique. As listed in Table I, the Hall effect measurements established a mobility value of 52 and 66 cm^2/Vs for 6H- and 3C-SiC samples, respectively. Both the samples doped with nitrogen exhibited n-type conductivity with carrier concertation values of 4.1×10^{17} and 2.9×10^{19} cm^{-3}, respectively. The doping concentration values indicated a higher dopant activation efficiency, at a lower activation temperature, in 3C-SiC as compared to 6H-SiC. The sheet resistance values, as listed in Table I, also reflected a lower carrier concentration in 6H-SiC as compared to 3C-SiC. Attempts will be made to further increase the doping concertation in 6H-SiC samples by increasing the thermal budget while ensuring minimal/no surface oxidation for device integration. The sheet resistance, activation anneal conditions, and piezoresistive properties will be correlated for high performance pressure and temperature sensor development on SiC wafers.

Table I. Electrical characteristics of ion-implanted 6H-SiC and 3C-SiC samples after activation annealing at 1450 °C and 1100 °C, respectively.

	Sheet Resistance (Ω/□)	**Hall mobility (cm^2/Vs)**	**Carrier Concentration (cm^{-3})**
6H-SiC	300-500	5.2×10^1	-4.1×10^{17}
3C-SiC/Si	55-75	6.6×10^1	-2.9×10^{19}

3.4 Device Fabrication and Piezoresistive Characterization

The 3C-SiC wafers (NOVASiC) were used for device processing and characterization. The n-type in-situ doped 3C-SiC wafers had a 0.78µm thick epitaxial layer with a doping concentration of 2×10^{18} cm^{-3}. A two-mask process was used to define the piezoresistors and process electrical contacts. The piezoresistors were defined on 3C-SiC wafers by patterning and dry-etching the SiC film. After the first photolithography step, the sensors were delineated in a positive resist followed by an ICP plasma etch. Sulfur hexafluoride (SF_6) with a 20% admixture of oxygen (O_2) was chosen as the etch gas. The plasma pressure during the etch process was 0.67 Pa and the substrates were maintained at 20°C by He backside cooling. RIE and ICP powers were optimized to obtain an etch profile close to 90 degrees. The resulting etch rate was close to 180 nm/min. The Au/Ti (100/100 nm) contact electrodes were fabricated on the piezoresistors through electron beam evaporation and lift-off processes as shown in Fig. 6(a). Al wires were bonded to the top Au/Ti electrodes to connect the sensing element with external wires for mechanical measurements.

To evaluate the mechanical characteristics of the piezoresistive sensors, a cantilever beam setup was used to measure strain by clamping the specimen on one end and loading on another. The mechanical load to the beam was realized by driving a micrometer spindle against the surface of the beam. The strain on the outer fiber of beam can be calculated according to the equation,

$$\varepsilon = \frac{3(l-x)}{2l^3}\delta h$$

where x is the distance of SiC sensor from the clamp, l the loading distance from the clamp, h the height of beam, δ the travel of micrometer, and ε the strain on the outer fiber of beam. The setup and method of measuring the strain was validated by using a steel beam with resistive strain gauge previously. In the present work, the Si beam dimensions were 60mm × 15mm × 1mm as described above. The SiC sensor and loading point were 14 mm and 47.5 mm away from the clamp, respectively.

The piezoresponse of the integrated sensors is shown in Fig. 6(b). The electrical resistance, R, of SiC sensor in a two-terminal configuration was measured using a Fluke multimeter. Aluminum foil served as shielding of setup to reduce the potential effect of external noises. The spindle travelled in a step size of 0.5 mm with a total distance of 2 mm. At each step, resistance readings were taken one minute after loading was applied to allow the system to stabilize. The resistances at specific loading level were captured in both the loading and unloading stages and then averaged. The data in Figure 6(b) are the results for the 3C-SiC sensor in the longitudinal direction of beam [100]. The in-situ doped 3C-SiC samples showed a linear response under bending induced microstrain. The gauge factor of the SiC sensor, defined as a ratio of the relative resistance change ($\Delta R/R$) to the strain ε, was calculated to be around 31.7. The observed results are promising for high temperature pressure sensor development exploiting doping induced piezoresistivity in SiC polytypes [16].

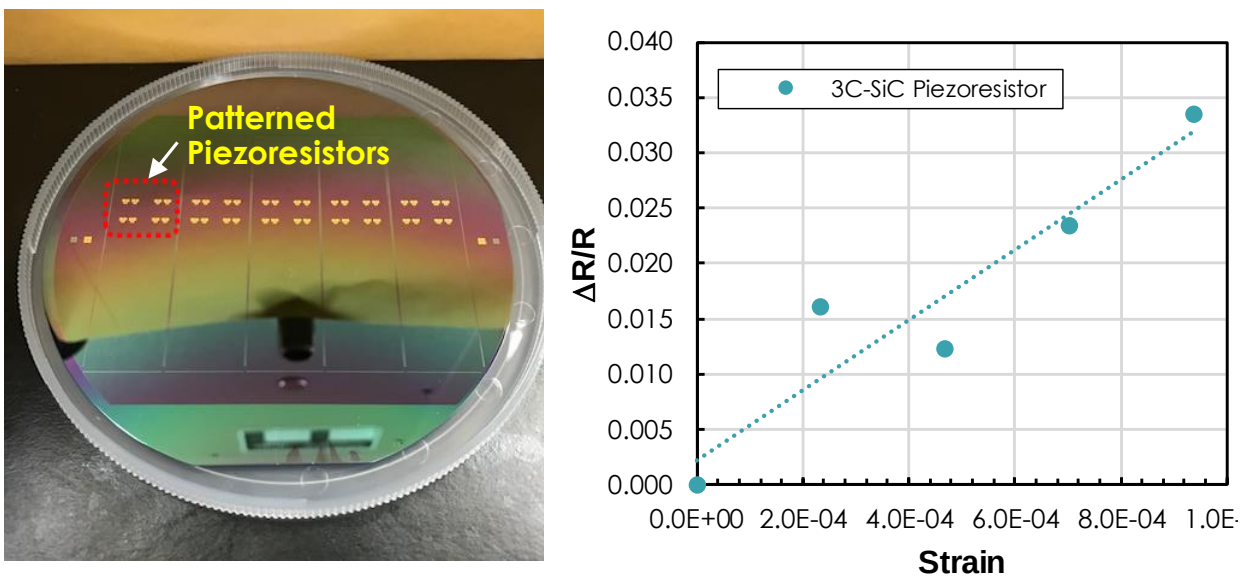

(a) (b)

Figure 6. (a) Patterned 3C-SiC wafer, and (b) the piezoresponse of the sensors under microstrain.

4 CONCLUSIONS

Ion-implanted and in-situ doped 6H- and 3C-SiC wafers are being investigated for piezoresistive sensor development. The ion-implantation profiles of these wafers were consistent with SRIM simulation as verified by SIMS and RBS measurements. The annealing setup and procedure were optimized to reduce wafer oxidation at temperatures higher than 1100°C. Both 6H- and 3C-SiC samples showed a high electrical conductivity after activation anneal which is critical to induce piezoresistivity and achieve a high gauge factor for high-temperature pressure sensor development. The device development was carried out on in-situ doped 3C-SiC wafers, and the patterned sensors show a strong piezoresponse under bending induced

microstrain. Detailed study is being conducted to analyze the impact of both p-type and n-type dopants on the SiC piezoresistive response.

5 ACKNOWLEDGEMENTS

The work was primarily sponsored by ORNL's LDRD funding. The submitted manuscript has been authored by a contractor of the U.S. Government under Contract DE-AC05-00OR22725. Accordingly, the U.S. Government retains a nonexclusive, royalty-free license to publish or reproduce the published form of this contribution, or allow others to do so, for U.S. Government purposes.

6 REFERENCES

1. K. Korsah, R. A. Kisner, C. L. Britton, P. Ramuhalli, D. W. Wootan, N. C. Anheier, A.A. Diaz, E. H. Hirt, R. B. Vilim, H.T. Chien, S. Bakhtiari, S. Sheen, S. Gopalsami, A. Heifetz, S.W. Tam, Y. Park, and B. R. Upadhyaya, "Assessment of Sensor Technologies for Advanced Reactors," *Proceedings of NPIC & HMIT*, San Francisco, CA, June 11-15, pp. 1115-1124 (2017).
2. "ORNL Reactor Technology Strategic Plan—Revision 1," ORNL/TM-2017/198, Nuclear Science and Engineering Directorate, Oak Ridge National Laboratory (2017).
3. N. G. Wright and A. B. Horsfall, "SiC sensors: a review," *J. Phys. D: Appl. Phys.*, **40**, pp. 6345-6354 (2007).
4. H-P Phan, D. V. Dao, K. Nakamura, S. Dimitrijev, and N-T Nguyen, "The Piezoresistive Effect of SiC for MEMS Sensors at High Temperatures: A Review," *Journal of Microelectromechanical Systems*, **24(6)**, pp. 1663-1677 (2015).
5. R. S. Okojie, D. Lukco, V. Nguyen, and E. Savrun, "4H-SiC Piezoresistive Pressure Sensors at 800 °C With Observed Sensitivity Recovery," *IEEE Electron Device Letters*, **36(2)**, pp. 174-176 (2015).
6. H-P Phan, T. Dinh, T. Kozeki, A. Qamar, T. Namazu, S. Dimitrijev, N-T Nguyen, and D. V. Dao, "Piezoresistive effect in p-type 3C-SiC at high temperatures characterized using Joule heating," *Scientific Reports*, **6**, 28499:1-9 (2016).
7. J. C. Doll and B. L. Pruitt, *Piezoresistor Design and Applications*, Springer, New York, NY, USA (2013).
8. E. M. Handy, M., Mulpuri V. Rao, O. W. Holland, P. H. Chi, K. A. Jones, M. A. Derenge, R. D. Vispute, and T. Venkatesan, "Al, B, and Ga Ion-Implantation Doping of SiC," *J. Electronic Materials*, **29 (11)**, pp. 1340-1345 (2000).
9. Y. Zhang, M. L. Crespillo, H. Xue, K. Jin, C. H. Chen, C. L. Fontana, J. T. Graham, and W. J. Weber, "New ion beam materials laboratory for materials modification and irradiation effects research," *Nucl. Instrum. Methods Phys. Res. B*, **338**, 19-30 (2014).
10. Y. Wang and M. A. Nastasi, eds. *Handbook of Modern Ion Beam Materials Analysis* (2nd ed.), Materials Research Society, Warrendale, Pennsylvania, USA (2010).
11. Y. Zhang, J. Lian, Z. Zhu, W.D. Bennett, L.V. Saraf, J. L. Rausch, C. A. Hendricks, R. C. Ewing, and W. J. Weber, "Response of strontium titanate to ion and electron irradiation," *Journal of Nuclear Materials*, **389**, pp. 303-310 (2009).
12. A. L. Ortiz, F. Sanchez-Bajo, F. L. Cumbrera, and F. Guiberteau, "X-ray powder diffraction analysis of a silicon carbide-based ceramic," *Materials Letters*, **49(2)**, pp. 137-145 (2001).

13. R. J. Iwanowski, K. Fronc, W. Paszkowicz, and M. Heinonen, "XPS and XRD study of crystalline 3C-SiC grown by sublimation method," *Journal of Alloys and Compounds*, **286(1-2)**, pp. 143-147 (1999).

14. L. Dong, G-S. Sun, J. Yu, L. Zheng, X-F. Liu, F. Zhang, G. G. Yan, X-G. Li, Z.G. Wang, and F. Yang, "Characterization of Obtuse Triangular Defects on 4H-SiC 4∘ off-Axis Epitaxial Wafers," *Chin. Phys. Lett.*, **30(9)**, 096105 (2013).

15. H. Wu, G. Sun, T. Yang, G. Yan, L. Wang, W. Zhao, and X. Liu, "Effect of annealing process on the surface roughness in multiple Al implanted 4H-SiC," *J. Semicond.*, **32(7)**, 072002 (2011).

16. D. V. Dao, H. P. Phan, A. Qamar, and T. Dinh, "Piezoresistive effect of p-type single crystalline 3C–SiC on (111) plane," *RSC Advances*, **6(26)**, pp. 21302-21307 (2016).